

Unraveling Atomically Irreversible Cation Migration in Sodium Layered Oxide Cathodes

Cheng Chen,^{||} Zhengping Ding,^{||} Zhen Han,^{||} Chaoping Liang, Xinyue Lan, Peng Wang,^{*} Peng Gao,^{*} and Weifeng Wei^{*}Cite This: *J. Phys. Chem. Lett.* 2020, 11, 5464–5470

Read Online

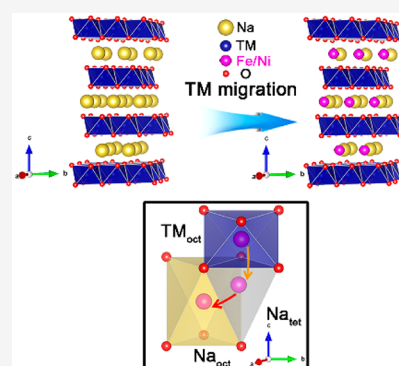
ACCESS |

Metrics & More

Article Recommendations

Supporting Information

ABSTRACT: Transition metal (TM)-based layered oxides NaTMO₂ (TM = Fe, Ni, Co, Mn, etc.) have been intensively pursued as high-capacity cathode materials for Na-ion batteries. Nevertheless, they still suffer from fast capacity loss and voltage decay, as a result of the layered structure instability upon extended electrochemical cycling. The mechanism underlying such instability remains poorly understood. Here we unravel the TM migrations and structural evolution of a quaternary NaNi_{0.3}Co_{0.12}Mn_{0.18}Fe_{0.4}O₂ compound during electrochemical cycling using atomic-resolution electron microscopy and associated spectroscopies. We discover successive migrations of TM ions to Na layers that account for structure and performance degradations. The Fe ions migrate into the interstices of both tetrahedra and octahedra of the layers; on the contrary, the Ni ions migrate predominantly in the octahedral ones, and the Mn and Co ions mostly remain in the TM layers. Direct atomic-level observations of the TM migration process upon cycling offer deep insight into designing high-capacity and long-life span cathode materials for sodium-ion batteries.



Transition metal (TM) layered oxides that consist of alternating layers of (Li/Na)O₆ octahedra and TMO₆ octahedra make up a class of important cathode materials for Li- and Na-ion batteries.^{1–6} As for Li-ion layered oxides, it is found that upon charging, Li ions are extracted from the Li layers to generate vacancies, to which the TM ions are prone to migrate, and the reverse migration of TM ions occurs as Li ions reinsert in the lattice during the subsequent discharge process.^{7–9} Irreversible TM migration behavior with structural distortion has been identified after extended cycles, characteristic of the partial occupancy of TM ions in the tetrahedral interstices and irreversible layered-to-spinel/rocksalt phase transitions.^{10,11} Specifically, utilizing atomic-resolution scanning transmission electron microscopy (STEM) imaging and electron energy loss spectroscopy (EELS) mapping, Yan et al. discovered the sequential migration of Ni, Co, and Mn to the Li layer in LiNi_{1/3}Mn_{1/3}Co_{1/3}O₂ upon electrochemical cycling, showing that Ni ions are prone to migrate, while Mn ions are relatively immobile when compared with Ni and Co ions and may act as a pillar to stabilize the layered structure.⁹

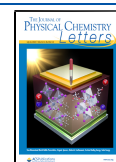
In contrast, TM migrations are generally regarded to be kinetically disfavored in Na-ion layered oxides due to the larger ionic radius of Na⁺ and are inhibited in some Na-ion layered oxides with P3-type or P2-type structure.¹² However, recent studies also reported that migration of the TM into the Na layer would occur in these Na-ion layered oxides.¹³ For instance, through the pair distribution function obtained from operando X-ray diffraction, Talaie et al. demonstrated the TM cation migration process and the positive effect of Ni substitution in the Mn/Fe-containing Na-ion layered ox-

ides.^{14,15} Kubota et al. investigated TM migration in NaCrO₂ cathodes through X-ray diffraction (XRD), X-ray absorption spectroscopy (XAS), and density functional theory (DFT) calculation.¹⁶ By comparing the experimental and simulated XRD patterns of the NaCrO₂ electrode at different states of charge (SOC), they found that Cr ions occupied both octahedral and tetrahedral sites in the Na layer when charged over 3.8 V corresponding to extraction of more than 0.5 Na in NaCrO₂, followed by the irreversible phase transition and the lattice contraction along the *c* axis. More recently, the migration of the TM between the TM layer and Na layer was verified in NaFeO₂ and Na_{0.8}Co_{0.4}Ti_{0.6}O₂ cathodes during the charge–discharge process, based on atomic-resolution STEM imaging and X-ray-based spectroscopy analyses.^{17,18} Therefore, severe capacity decay of these layered oxides is considered to be related to the irreversible structural transition at the deep charge state, including migration of the TM and incorporation of the solvent molecule into the Na layer.^{19,20} In the latter case, surface modification has been proposed to effectively protect the cathode particle from electrolyte attacks,^{21–23} resulting in better reversibility of Na⁺ motion, but such strategies fail to mitigate TM migration. In-depth

Received: April 28, 2020

Accepted: June 15, 2020

Published: June 15, 2020



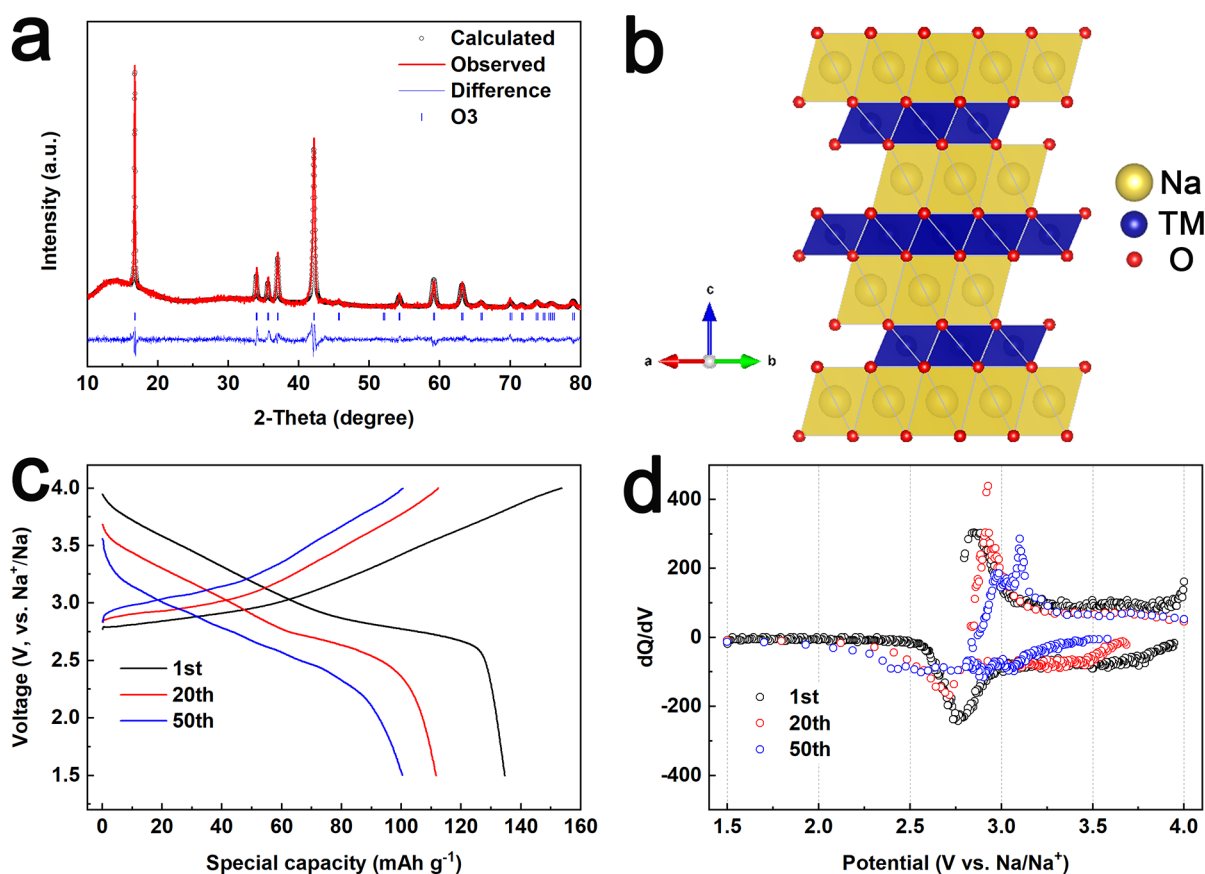


Figure 1. (a) Powder XRD pattern and Rietveld plot of pristine $\text{NaNi}_{0.3}\text{Co}_{0.12}\text{Mn}_{0.18}\text{Fe}_{0.4}\text{O}_2$ (NCMF) material. (b) Schematic structure for the O3- NaTMO_2 phase. (c) Charge–discharge voltage profiles and (d) corresponding dQ/dV curves of the NCMF cathode during cycling in the voltage range of 1.5–4.0 V vs Na^+/Na .

theoretical studies suggested the preferential migration pathway from Fe_{oct} to Na_{oct} through the tetrahedron site in the Na layer (Na_{tet}), and the occupancy of both the tetrahedral and octahedral sites of the Na layer to generate a spinel-like structure that impedes Na diffusion.²⁴ In general, TM migration would block the channels of Na^+ ions and then cause a reduced diffusion kinetic.²⁵ In addition, the valence of the TM ion is usually higher than +3 near the end of Na^+ -ion deintercalation,¹³ and such strong electrostatic repulsion induced by these TM ions restricts the reinsertion of the Na^+ ion in the subsequent discharge progress, perhaps leading to a decrease in the interslab space, as a result of growing electrostatic attraction between TM and O layers. Li, Vassilaras, and co-workers proposed that partial substitution to form ternary and quaternary TM-based sodium layered oxides is effective for alleviating TM migration and associated structure and performance degradation.^{26,27} In such cases, a few important questions remain unanswered. (1) Which TM ions preferentially migrate to the Na layer during electrochemical cycling, and (2) in what interstitial sites are the migrated TM ions trapped? Direct observation at the atomic scale is therefore required to fully understand the migration behavior of multiple TM species and the degradation mechanism of Na-ion layered oxides.

In this work, we investigated the TM migrations and structural evolution of a quaternary $\text{NaNi}_{0.3}\text{Co}_{0.12}\text{Mn}_{0.18}\text{Fe}_{0.4}\text{O}_2$ (NCMF) layered oxide using aberration-corrected STEM imaging and associated EELS/energy dispersion spectroscopy (EDS). For the first time, we visualized the migration of TM

ions to Na layers upon cycling in atomic-resolution EDS elemental mapping. Fe and Ni ions preferentially migrate into the Na layer, inducing structural transition and degrading electrochemical performance. Our findings provide an atomic-level understanding of the mechanism of the irreversible TM migration and provide insights into designing high-capacity and long-life span Na intercalation cathode materials.

The stoichiometric $\text{NaNi}_{0.3}\text{Co}_{0.12}\text{Mn}_{0.18}\text{Fe}_{0.4}\text{O}_2$ (NCMF) material, as confirmed by inductively coupled plasma-optical emission spectrometry (ICP-OES) (Table S1), was synthesized via a coprecipitation and solid-state method as reported in our previous works.^{28,29} Typical scanning electron microscopy (SEM) images demonstrate its aggregated spherical morphology and homogeneous size distribution (Figure S1). Figure 1a and Table S2 show the XRD pattern and Rietveld refinement of pristine material with all diffraction peaks that can be well indexed to an O3-type structure with space group $R\bar{3}m$, as schematically illustrated in Figure 1b. The electrochemical performance of the NCMF material was evaluated at a rate of 0.1 C in the potential range of 1.5–4.0 V. As shown in panels c and d of Figure 1 and Figure S2, continuous performance degradation, including specific capacity decay and voltage fading (or increased polarization), can be clearly observed in the charge–discharge profiles and corresponding differential capacity versus equivalent voltage (dQ/dV) profiles (Figure 1c,d). The performance degradation is closely related to the structural irreversibility upon electrochemical cycling, and the underlying atomic-scale

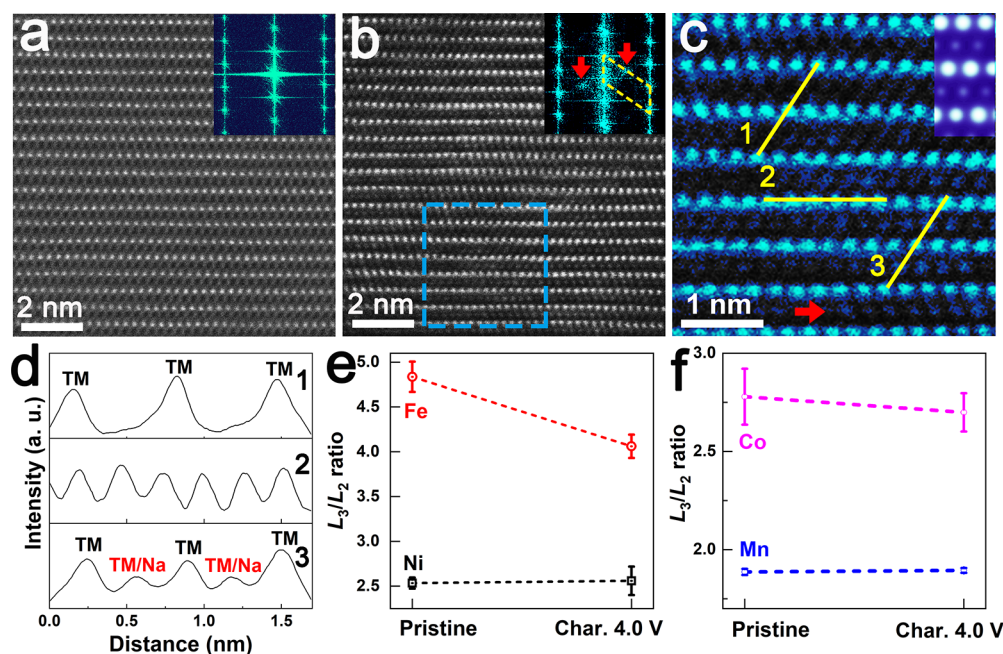


Figure 2. (a) Typical STEM-HAADF image and corresponding FFT pattern (inset) for a pristine NCMF cathode along the [100] zone axis. (b) STEM-HAADF image and corresponding FFT pattern (inset) for the NCMF cathode charged to 4.0 V along the [100] zone axis showing TM migration. (c) Enlarged STEM-HAADF image taken from panel b and simulated HAADF image with 40% of the TM ions having migrated to the Na layers (inset) by QSTEM. (d) Line profiles taken along yellow lines in the STEM-HAADF image in panel c. (e and f) White-line ratios (L_3/L_2) for pristine and charged NCMF cathode materials.

process in cycled cathode materials will be investigated in the following sections.

The cross-sectional STEM samples of the pristine and charged NCMF cathodes were prepared using the focused ion beam (FIB) lift-out technique and analyzed using atomic-resolution high-angle annular dark field (HAADF) and annular bright field (ABF) imaging and EELS. Figure S3 shows the typical low-magnification STEM-HAADF image and SAED pattern for the pristine NCMF cathode prepared by the FIB lift-out technique. As shown in Figure S3a, the NCMF sample consisted of 150–500 nm aggregated nanoparticles. To obtain the atomic-resolution HAADF and EDS image, the zone axis of the FIBed sample is tilted to the [100] axis. The corresponding SAED pattern is shown in Figure S3b. The STEM-HAADF image of the pristine NCMF cathode along the [100] zone axis shows that all of the TM cations with bright dot contrast reside in the TM layers, and Na ions with much weaker dot contrast are hardly observed in the Na layers,³⁰ demonstrating a well-ordered layered structure (Figure 2a). In contrast, the STEM-HAADF images of the charged NCMF cathode along the [100] zone axis exhibit distinct bright dot contrast between TM slabs (red arrow in Figure 2c), suggesting migration of the TM into the Na layers, which is evidenced by the extra diffraction spots in the fast Fourier transform (FFT) pattern (red arrows in the inset of Figure 2b). A corresponding O3-NaTMO₂ structure with 40% of the TM cations having migrated to the Na layers was used as a model to simulate the contrast in Figure 2c by QSTEM software (inset of Figure 2c). Also, three line profiles taken from Figure 2c confirm the migration of the TM into the Na layers, as shown in Figure 2d. The STEM-ABF images and corresponding line profiles of the charged NCMF cathode (Figure S4) also provide the direct visualization of the behavior of TM migration.

EELS spectra of Ni, Co, Mn, and Fe *L*-edges taken from the pristine and charged NCMF cathodes are compared in Figure S5. No apparent chemical shift can be observed for these TM *L*-edges for the NCMF cathodes before or after charging (Figure S5). To appreciate the variations of the oxidation state of 3d TM ions, the white-line ratio (L_3/L_2) method has been well established in the literature.^{31–33} Here, the L_3/L_2 white-line ratios based on the corresponding EELS spectra were calculated to understand the variation of the oxidation state of 3d TM ions upon electrochemical charging (Figure 2). Note that although Co ions are generally considered to be electrochemically inactive upon charging and discharging, a change of 2.9% in the white-line ratio of Co is observed in Figure 2f. Nevertheless, compared to the 19.1% change for Fe, the subtle change for Co suggests that the charge capacity of the cathode materials is mainly attributed to Fe oxidation/reduction. It is evident that the L_3/L_2 ratios of Fe ions experience remarkable changes for the NCMF cathode upon charging, while those of Ni, Co, and Mn ions remain almost invariant, as plotted in panels e and f of Figure 2. This trend suggests that the oxidation state of Fe ions increases to a higher valence state and the charge capacity of the NCMF cathode is mainly attributed to Fe oxidation.^{34–36}

Dumbbell defect formation can be assisted by TM migration upon Na⁺ deintercalation from the crystal structure;¹² therefore, DFT calculations are performed to compare the formation energies for different TM–Na dumbbell structures (migration of the TM from TM_{oct} to Na_{tet} interstices). As shown in Figure S6, the dumbbell formation energies are approximately 0.2 eV for Fe and Ni ions while those for Mn and Co ions are as high as 1.20 and 1.76 eV, respectively. Nevertheless, due to the small amount of migrated TM species, atomic-resolution element mappings to differentiate the sequential TM migration process are difficult to capture from

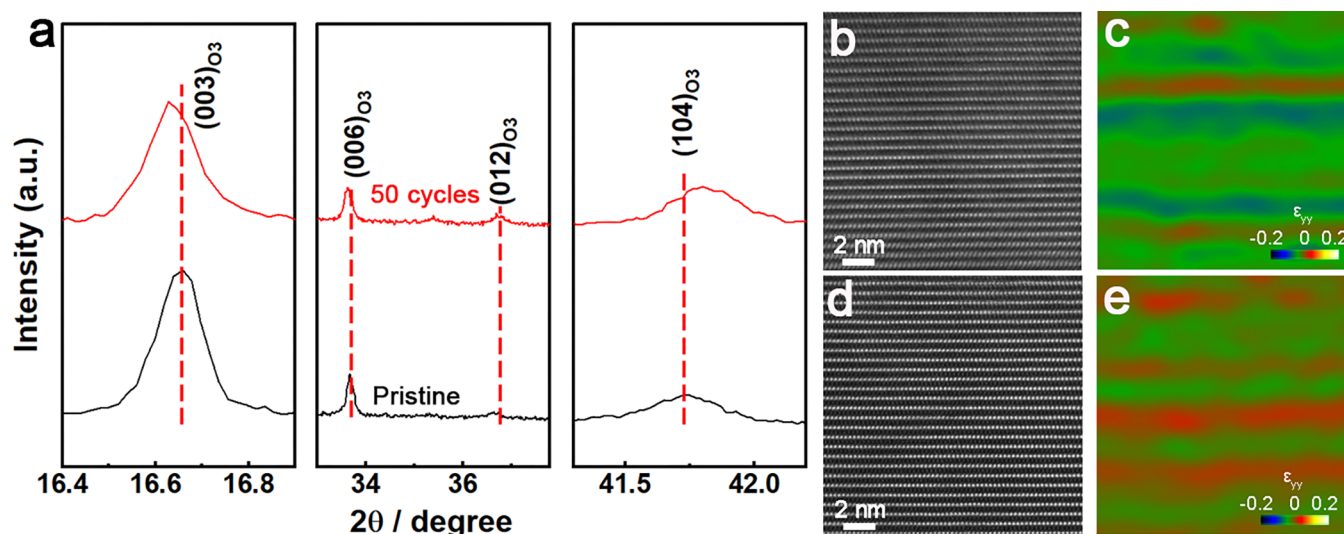


Figure 3. (a) Powder X-ray diffraction patterns taken from pristine and cycled NCMF cathodes. (b and c) Atomic-resolution HAADF image and GPA image, respectively, for the pristine NCMF cathode. (d and e) Atomic-resolution HAADF image and GPA image, respectively, for the cycled NCMF cathode.

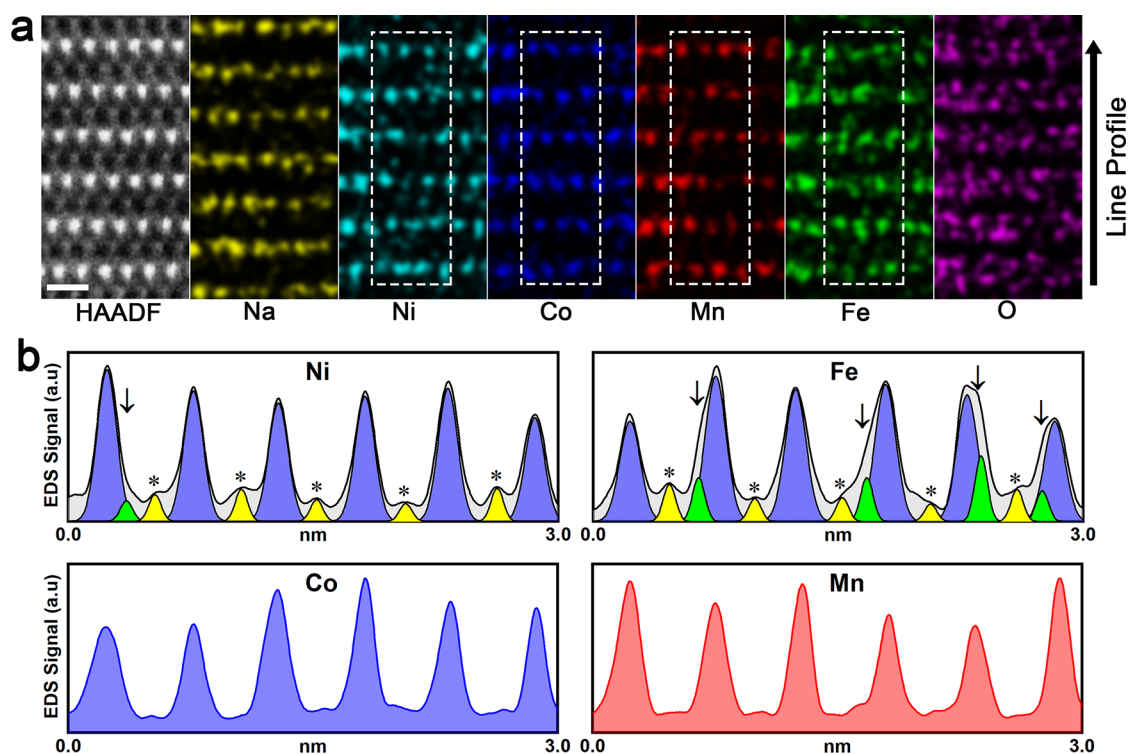


Figure 4. (a) Atomic-resolution STEM-HAADF image and EDS elemental mappings of the NCMF cathode after 50 cycles along the [100] zone axis. The scale bars in panel a are 0.5 nm. (b) EDS mapping line profiles of Ni, Fe, Co, and Mn acquired from the white rectangles in panel a. Yellow peaks indicate cation octahedra on the Na layer (marked with asterisks), and green peaks indicate cation tetrahedra on the Na layer (marked with arrowheads).

the charged NCMF materials. More structural analyses are therefore conducted on the NCMF cathode material after extended cycles.

Figure 3a compares the XRD pattern for the cycled NCMF cathode after 50 cycles with the XRD pattern of the pristine one. It is evident that, after 50 cycles, the pure O3 phase is well maintained. However, the (003) reflection shifts to a smaller 2θ angle and the (104) reflections shift to larger 2θ angles, indicating the expanded interlayer distance along the c axis and

the contractive a - b plane for the cycled NCMF cathode (see Rietveld refinement results in Table S3). These observations can be attributed to less reinsertion of Na⁺ and significant structural irreversibility induced by TM migration during the repetitive O3-P3 phase transition upon cycling. In addition, geometric phase analysis (GPA) based on atomic STEM-HAADF images was also implemented to study the internal strain and structural distortion in both pristine and cycled NCMF cathode materials (Figure 3b-e).^{37,38} Evidently, the

cycled material exerts an alternating strain distribution along the *c* axis, i.e., fluctuating interlayer distance, as compared with the relatively smaller and relatively uniform internal strain distribution in the pristine material.

To address the key questions about which TM ions are prone to migration into Na layers and which interstitial sites of the Na layers are occupied by the migrated TM ions, atomic-resolution STEM-EDS mapping was employed to directly correlate the structural evolution with the spatial distribution of Ni, Co, Mn, and Fe. Figure 4a shows the atomic-resolution STEM-HAADF image of a typical area in cycled NCMF and corresponding EDS elemental mappings, taken from the green rectangle in Figure S7. The atomic EDS elemental mappings confirm that the spatial distribution of Na, O, and TM ions is distinguished and reliable. Apparently, Mn and Co ions mostly reside in the TM layer, and Ni and Fe cations deviated from a well-ordered layered structure to different degrees; however, the deviation of the Fe element distribution is drastic, indicative of preferential migration of Fe from the TM layer into the Na layer when most of the Na ions were extracted from the lattice. The line profiles of EDS mapping images of TM ions along the [001] direction (Figure 4b) further prove that both tetrahedral and octahedral interstices of the Na layer are occupied by the migrated Fe cations, whereas the migrated Ni ions predominantly reside on the octahedral interstices of the Na layer after cycling. Thus, the spatial distribution of Ni, Co, Mn, and Fe ions essentially indicates the diverse tendency of migration of the TM from the TM layer to the Na layer, highlighting a sequential migration process of Fe, Ni, Co, and Mn ions. With respect to structural stability, the stability of the Ni ion is better than that of the Fe ion, while Mn and Co ions are the most stable TM species and play an important role in stabilizing the layered structure.

Collectively, these experimental and theoretical data confirm that the irreversible structural change is closely related to TM migration, which is a process of preferential hopping of TM ions to the Na layer. Mn and Co ions are observed to be resistant to migration during electrochemical cycling and play an important role in stabilizing the crystal structure. Other TM ions, especially Fe, are prone to migrate into the Na layer. It is well-known that migration of the TM between adjacent octahedra must proceed along the $\text{TM}_{\text{oct}}-\text{Na}_{\text{tet}}-\text{Na}_{\text{oct}}$ path due to TMO_6 octahedral edge sharing with the alkali metal octahedron, and the maximum energy barrier along the TM migration pathway must be overcome when TMs diffuse through the oxygen triangle between the TM and the alkali metal layer.³⁹ When most of the $\text{Fe}^{3+/4+}$ redox ions are utilized, Fe ions would become Jahn–Teller (JT) active upon desodiation, and then the strong JT effect would provide the structural distortion needed for Fe migration and collectively reduce the energy barrier needed for Fe to pass through the oxygen triangle.¹⁷ Specifically, both tetrahedral and octahedral interstices of the Na layers are occupied by the migrated Fe ions after cycling, as a result of electrostatic interaction, which has a detrimental impact on the reinsertion of Na^+ and leads to gradual capacity loss and poorer rate performance.

In summary, we examined the TM migration and structural evolution of a quaternary $\text{NaNi}_{0.3}\text{Co}_{0.12}\text{Mn}_{0.18}\text{Fe}_{0.4}\text{O}_2$ layered oxide using aberration-corrected STEM imaging and associated EELS/EDS analyses. Atomic-resolution EDS elemental mapping of the cycled material reveals the successive migration of Fe and Ni to the Na layer that leads to the degradation of structure and performance. Our experimental evidence

provides some new insights into the atomic-scale working mechanism for the structural instability in NaTMO_2 layered oxides with multiple TM species, inspiring the subsequent material design and property optimization for high-performance TM-based NaTMO_2 cathode materials for Na-ion batteries.

■ ASSOCIATED CONTENT

Supporting Information

The Supporting Information is available free of charge at <https://pubs.acs.org/doi/10.1021/acs.jpcllett.0c01285>.

Additional experimental details, crystallographic tables, and details of XRD and DFT calculations (PDF)

■ AUTHOR INFORMATION

Corresponding Authors

Weifeng Wei – State Key Laboratory of Powder Metallurgy, Central South University, Changsha, Hunan 410083, People's Republic of China; orcid.org/0000-0002-3088-6549; Email: weifengwei@csu.edu.cn

Peng Gao – International Center for Quantum Materials and Electron Microscopy Laboratory, School of Physics, Peking University, Beijing 100871, People's Republic of China; orcid.org/0000-0003-0860-5525; Email: p-gao@pku.edu.cn

Peng Wang – National Laboratory of Solid State Microstructures, Jiangsu Key Laboratory of Artificial Functional Materials, College of Engineering and Applied Sciences and Collaborative Innovation Center of Advanced Microstructures, Nanjing University, Nanjing 210093, China; Email: wangpeng@nju.edu.cn

Authors

Cheng Chen – State Key Laboratory of Powder Metallurgy, Central South University, Changsha, Hunan 410083, People's Republic of China

Zhengping Ding – International Center for Quantum Materials and Electron Microscopy Laboratory, School of Physics, Peking University, Beijing 100871, People's Republic of China; orcid.org/0000-0001-5275-5905

Zhen Han – National Laboratory of Solid State Microstructures, Jiangsu Key Laboratory of Artificial Functional Materials, College of Engineering and Applied Sciences and Collaborative Innovation Center of Advanced Microstructures, Nanjing University, Nanjing 210093, China

Chaoping Liang – State Key Laboratory of Powder Metallurgy, Central South University, Changsha, Hunan 410083, People's Republic of China

Xinyue Lan – State Key Laboratory of Powder Metallurgy, Central South University, Changsha, Hunan 410083, People's Republic of China

Complete contact information is available at: <https://pubs.acs.org/doi/10.1021/acs.jpcllett.0c01285>

Author Contributions

^{||}C.C., Z.D., and Z.H. contributed equally to this work.

Notes

The authors declare no competing financial interest.

■ ACKNOWLEDGMENTS

This work was supported by the National Natural Science Foundation of China (51304248, 11874199, 51971250,

51672007, and 11974023), the National Key Research and Development Program of China (Grant 2018YFB010400), SAFEA: High-End Foreign Experts Project (Grant B06020), the Key R&D Program of Guangdong Province (2018B030327001 and 2018B010109009), the China Postdoctoral Science Foundation (2019M650333), the International Science and Technology Cooperation Program of China (2014DFE00200), the Open Project (621011913), the Fundamental Research Funds for the Central Universities (020514380224), the Innovation Program of Central South University (2020CX007), and the State Key Laboratory of Powder Metallurgy at Central South University. P. G. gratefully acknowledges the support from the National Program for Thousand Young Talents of China and the "2011 Program" Peking-Tsinghua-IOP Collaborative Innovation Center of Quantum Matter.

REFERENCES

- (1) Delmas, C.; Fouassier, C.; Hagenmuller, P. Structural Classification and Properties of the Layered Oxides. *Physica B+C (Amsterdam)* **1980**, *99*, 81–85.
- (2) Whittingham, M. S. Lithium batteries and cathode materials. *Chem. Rev.* **2004**, *104*, 4271–4301.
- (3) Xiang, X.; Zhang, K.; Chen, J. Recent Advances and Prospects of Cathode Materials for Sodium-Ion Batteries. *Adv. Mater.* **2015**, *27*, 5343–64.
- (4) Kang, K. S.; Meng, Y. S.; Breger, J.; Grey, C. P.; Ceder, G. Electrodes with high power and high capacity for rechargeable lithium batteries. *Science* **2006**, *311*, 977–980.
- (5) Yabuuchi, N.; Yoshii, K.; Myung, S.-T.; Nakai, I.; Komaba, S. Detailed Studies of a High-Capacity Electrode Material for Rechargeable Batteries, $\text{Li}_2\text{MnO}_3\text{-LiCo}_{1/3}\text{Ni}_{1/3}\text{Mn}_{1/3}\text{O}_2$. *J. Am. Chem. Soc.* **2011**, *133*, 4404–4419.
- (6) Sharma, N.; Gonzalo, E.; Pramudita, J. C.; Han, M. H.; Brand, H. E. A.; Hart, J. N.; Pang, W. K.; Guo, Z.; Rojo, T. The Unique Structural Evolution of the O3-Phase $\text{Na}_{2/3}\text{Fe}_{2/3}\text{Mn}_{1/3}\text{O}_2$ during High Rate Charge/Discharge: A Sodium-Centred Perspective. *Adv. Funct. Mater.* **2015**, *25*, 4994–5005.
- (7) Gu, M.; Belharouak, I.; Zheng, J.; Wu, H.; Xiao, J.; Genc, A.; Amine, K.; Thevuthasan, S.; Baer, D. R.; Zhang, J.-G.; Browning, N. D.; Liu, J.; Wang, C. Formation of the Spinel Phase in the Layered Composite Cathode Used in Li-Ion Batteries. *ACS Nano* **2013**, *7*, 760–767.
- (8) Lu, P.; Yuan, R. L.; Ihlefeld, J. F.; Spoecker, E. D.; Pan, W.; Zuo, J. M. Fast Atomic-Scale Chemical Imaging of Crystalline Materials and Dynamic Phase Transformations. *Nano Lett.* **2016**, *16*, 2728–2733.
- (9) Yan, P.; Zheng, J.; Zhang, J. G.; Wang, C. Atomic Resolution Structural and Chemical Imaging Revealing the Sequential Migration of Ni, Co, and Mn upon the Battery Cycling of Layered Cathode. *Nano Lett.* **2017**, *17*, 3946–3951.
- (10) Sathiyaraj, M.; Abakumov, A. M.; Foix, D.; Rousse, G.; Ramesha, K.; Saubanere, M.; Doublet, M. L.; Vezin, H.; Laisa, C. P.; Prakash, A. S.; Gonbeau, D.; Van Tendeloo, G.; Tarascon, J. M. Origin of voltage decay in high-capacity layered oxide electrodes. *Nat. Mater.* **2015**, *14*, 230–238.
- (11) Gao, Y.; Ma, J.; Wang, Z.; Lu, G.; Chen, L. Vacancy-induced MnO_6 distortion and its impacts on structural transition of Li_2MnO_3 . *Phys. Chem. Chem. Phys.* **2017**, *19*, 7025–7031.
- (12) Kim, S.; Ma, X.; Ong, S. P.; Ceder, G. A comparison of destabilization mechanisms of the layered Na_xMO_2 and Li_xMO_2 compounds upon alkali de-intercalation. *Phys. Chem. Chem. Phys.* **2012**, *14*, 15571–8.
- (13) Bo, S.-H.; Li, X.; Toumar, A. J.; Ceder, G. Layered-to-rock-salt transformation in desodiated Na_xCrO_2 ($x < 0.4$). *Chem. Mater.* **2016**, *28*, 1419–1429.
- (14) Talaie, E.; Duffort, V.; Smith, H. L.; Fultz, B.; Nazar, L. F. Structure of the high voltage phase of layered $\text{P2-Na}_{2/3-z}[\text{Mn}_{1/2}\text{Fe}_{1/2}]$ - O_2 and the positive effect of Ni substitution on its stability. *Energy Environ. Sci.* **2015**, *8*, 2512–2523.
- (15) Talaie, E.; Kim, S. Y.; Chen, N.; Nazar, L. F. Structural evolution and redox processes involved in the electrochemical cycling of $\text{P2-Na}_{0.67}[\text{Mn}_{0.66}\text{Fe}_{0.20}\text{Cu}_{0.14}]\text{O}_2$. *Chem. Mater.* **2017**, *29*, 6684–6697.
- (16) Kubota, K.; Ikeuchi, I.; Nakayama, T.; Takei, C.; Yabuuchi, N.; Shiiba, H.; Nakayama, M.; Komaba, S. New insight into structural evolution in layered NaCrO_2 during electrochemical sodium extraction. *J. Phys. Chem. C* **2015**, *119*, 166–175.
- (17) Li, Y.; Gao, Y.; Wang, X.; Shen, X.; Kong, Q.; Yu, R.; Lu, G.; Wang, Z.; Chen, L. Iron migration and oxygen oxidation during sodium extraction from NaFeO_2 . *Nano Energy* **2018**, *47*, 519–526.
- (18) Zhang, X.; Guo, S.; Liu, P.; Li, Q.; Xu, S.; Jiang, K.; He, P.; Chen, M.; Wang, P.; Zhou, H. Capturing Reversible Cation Migration in Layered Structure Materials for Na-Ion Batteries. *Adv. Energy Mater.* **2019**, *9*, 1900189.
- (19) Kubota, K.; Asari, T.; Yoshida, H.; Yabuuchi, N.; Shiiba, H.; Nakayama, M.; Komaba, S. Understanding the structural evolution and redox mechanism of a $\text{NaFeO}_2\text{-NaCoO}_2$ solid solution for sodium-ion batteries. *Adv. Funct. Mater.* **2016**, *26*, 6047–6059.
- (20) Komaba, S.; Yabuuchi, N.; Nakayama, T.; Ogata, A.; Ishikawa, T.; Nakai, I. Study on the reversible electrode reaction of $\text{Na}_{1-x}\text{Ni}_{0.5}\text{Mn}_{0.5}\text{O}_2$ for a rechargeable sodium-ion battery. *Inorg. Chem.* **2012**, *51*, 6211–6220.
- (21) Jo, C.-H.; Jo, J.-H.; Yashiro, H.; Kim, S.-J.; Sun, Y.-K.; Myung, S.-T. Bioinspired surface layer for the cathode material of high-energy-density sodium-ion batteries. *Adv. Energy Mater.* **2018**, *8*, 1702942.
- (22) Hwang, J.-Y.; Myung, S.-T.; Choi, J.; Yoon, C.; Yashiro, H.; Sun, Y.-K. Resolving the degradation pathways of the O3-type layered oxide cathode surface through the nano-scale aluminum oxide coating for high-energy density sodium-ion batteries. *J. Mater. Chem. A* **2017**, *5*, 23671–23680.
- (23) Hwang, J.-Y.; Yu, T.-Y.; Sun, Y.-K. Simultaneous MgO coating and Mg doping of $\text{Na Ni}_{0.5}\text{Mn}_{0.5}\text{O}_2$ cathode: facile and customizable approach to high-voltage sodium-ion batteries. *J. Mater. Chem. A* **2018**, *6*, 16854–16862.
- (24) Li, X.; Wang, Y.; Wu, D.; Bo, S.-H.; Ceder, G. Jahn–Teller Assisted Na Diffusion for High Performance Na Ion Batteries. *Chem. Mater.* **2016**, *28*, 6575–6583.
- (25) Yabuuchi, N.; Yano, M.; Yoshida, H.; Kuze, S.; Komaba, S. Synthesis and electrode performance of O3-type $\text{NaFeO}_2\text{-NaNi}_{1/2}\text{Mn}_{1/2}\text{O}_2$ solid solution for rechargeable sodium batteries. *J. Electrochem. Soc.* **2013**, *160*, A3131–A3137.
- (26) Li, X.; Wu, D.; Zhou, Y.-N.; Liu, L.; Yang, X.-Q.; Ceder, G. O3-type $\text{Na}(\text{Mn}_{0.25}\text{Fe}_{0.25}\text{Co}_{0.25}\text{Ni}_{0.25})\text{O}_2$: A quaternary layered cathode compound for rechargeable Na ion batteries. *Electrochem. Commun.* **2014**, *49*, 51–54.
- (27) Vassilaras, P.; Toumar, A. J.; Ceder, G. Electrochemical properties of $\text{NaNi}_{1/3}\text{Co}_{1/3}\text{Fe}_{1/3}\text{O}_2$ as a cathode material for Na-ion batteries. *Electrochem. Commun.* **2014**, *38*, 79–81.
- (28) Chen, C.; Han, B.; Lin, G.; Huang, Q.; Zhao, S.; Zhang, D.; Ma, C.; Ivey, D.; Wei, W. Electrochemical Property-Structure Correlation for Ni-Based Layered Na-Ion Cathodes. *ACS Appl. Mater. Interfaces* **2018**, *10*, 28719–28725.
- (29) Chen, C.; Han, Z.; Chen, S.; Qi, S.; Lan, X.; Zhang, C.; Chen, L.; Wang, P.; Wei, W. Core-Shell Layered Oxide Cathode for High-Performance Sodium-Ion Batteries. *ACS Appl. Mater. Interfaces* **2020**, *12*, 7144–7152.
- (30) Lu, X.; Wang, Y.; Liu, P.; Gu, L.; Hu, Y. S.; Li, H.; Demopoulos, G. P.; Chen, L. Direct imaging of layered O3- and P2- $\text{Na}_x\text{Fe}_{1/2}\text{Mn}_{1/2}\text{O}_2$ structures at the atomic scale. *Phys. Chem. Chem. Phys.* **2014**, *16*, 21946–52.
- (31) Graetz, J.; Ahn, C. C.; Ouyang, H.; Rez, P.; Fultz, B. White lines and d-band occupancy for the 3d transition-metal oxides and lithium transition-metal oxides. *Phys. Rev. B: Condens. Matter Mater. Phys.* **2004**, *69*, 235103.
- (32) Schmid, H. K.; Mader, W. Oxidation states of Mn and Fe in various compound oxide systems. *Micron* **2006**, *37*, 426–432.

(33) Tan, H.; Verbeeck, J.; Abakumov, A.; Van Tendeloo, G. Oxidation state and chemical shift investigation in transition metal oxides by EELS. *Ultramicroscopy* **2012**, *116*, 24–33.

(34) Koyama, Y.; Mizoguchi, T.; Ikeno, H.; Tanaka, I. Electronic Structure of Lithium Nickel Oxides by Electron Energy Loss Spectroscopy. *J. Phys. Chem. B* **2005**, *109*, 10749–10755.

(35) Wang, Z. L.; Yin, J. S.; Jiang, Y. D. EELS analysis of cation valence states and oxygen vacancies in magnetic oxides. *Micron* **2000**, *31*, 571–580.

(36) Vassilaras, P.; Kwon, D.-H.; Dacek, S. T.; Shi, T.; Seo, D.-H.; Ceder, G.; Kim, J. C. Electrochemical properties and structural evolution of O3-type layered sodium mixed transition metal oxides with trivalent nickel. *J. Mater. Chem. A* **2017**, *5*, 4596–4606.

(37) Hýtch, M.J.; Snoeck, E.; Kilaas, R. Quantitative measurement of displacement and strain fields from HREM micrographs. *Ultramicroscopy* **1998**, *74*, 131–146.

(38) Rouviere, J. L.; Sarigiannidou, E. Theoretical discussions on the geometrical phase analysis. *Ultramicroscopy* **2005**, *106*, 1–17.

(39) Zhang, Y.; Kim, S.; Feng, G.; Wang, Y.; Liu, L.; Ceder, G.; Li, X. The Interaction between Cu and Fe in P2-Type Na_xTMO_2 Cathodes for Advanced Battery Performance. *J. Electrochem. Soc.* **2018**, *165*, A1184–A1192.